ChemComm

COMMUNICATION

View Article Online
View Journal | View Issue

Cite this: *Chem. Commun.*, 2025, **61**, 3860

Received 22nd November 2024,
Accepted 6th February 2025

DOI: 10.1039/d4cc06196a

rsc.li/chemcomm

Relating norbornene composition-to-reactivity for thiol–ene photopolymerizations and 3D printing†

Yutong Liu,[a] Henry L. Cater,[a] Elizabeth A. Recker[b] and Zachariah A. Page *[ab]

Structure–reactivity relationships for an array of norbornene derivatives in light-initiated thiol–ene reactions were unveiled using real-time Fourier-transform infrared (FTIR) spectroscopy. Guided by these results, poly(*N*-hydroxyethyl acrylamide) was functionalized with *exo*-norbornenemide and used in digital light processing (DLP) 3D printing of biomimetic hydrogels.

Photo-induced thiol–ene "click" chemistry has been widely used in polymer functionalization,[1] coatings,[2] and biomolecule patterning[3] owing to its high speed, yields, and selectivity. Its metal-free nature and oxygen insensitivity make it well-suited for emerging technologies in 3D printing[4] and tissue engineering.[5] Contemporary light-based 3D printing techniques, such as digital light processing (DLP), predominantly use acrylic resins given their rapid curing upon exposure to light. However, these polymerizations typically proceed by an uncontrolled free-radical chain-growth mechanism, forming heterogeneous networks with compromised mechanical integrity. In contrast, thiol–ene reactions undergo a step-growth polymerization mechanism, providing more uniform polymer networks and enhanced mechanical properties as a result (*e.g.*, higher strength and toughness).[6] Yet, step-growth kinetics delay gelation relative to analogous chain-growth processes, hampering their implementation in DLP 3D printing.

In a typical thiol–ene reaction, a thiyl radical is generated upon light irradiation in the presence of a photo-initiator (Fig. 1A). The thiyl radical adds across an alkene to generate a carbon-centered radical, which can undergo either step- or chain-growth. The chemical structure of the alkene influences radical propagation kinetics, including thiyl radical addition to alkene, k_a, along with carbon-centered radical chain-transfer to thiol, k_{CT}, and addition to alkene (*i.e.*, chain-growth), k_{CG}.[7] Bowman,[8] Hoyle[9] and their coworkers have conducted systematic experimental studies on thiol–ene reactivity for various alkenes, revealing that acrylates exhibit predominantly chain-growth kinetics ($k_{CG} >> k_{CT}$), whilst norbornene (Nb) and allyl ether groups display ~pure step-growth kinetics ($k_{CG} << k_{CT}$). Building on this body of work, Coffey and coworkers[6] evaluated radical-initiated thiol–ene kinetics *via* computation, again showing how alkene structure impacts reactivity.

Based on these prior studies, Nb stands out for its high radical thiol–ene reactivity and clean step-growth mechanism,[7,9,10] making it an ideal candidate for photocurable applications, such as forming hydrogels[11] *via* 3D printing.[12] However, Nb functionality is diverse,[13] with examples of hydrocarbon,[14] ester-,[15–17] amide-,[18,19] and imide[20] linkages in prepolymers for light-initiated network formation. Despite this variety and the known influence of alkene composition on radical thiol–ene kinetics, a detailed study to elucidate structure–reactivity relationships in Nb derivatives is lacking.

Here, we fill this gap in knowledge by monitoring thiol–ene kinetics for ten distinct Nb derivatives *via* real-time Fourier

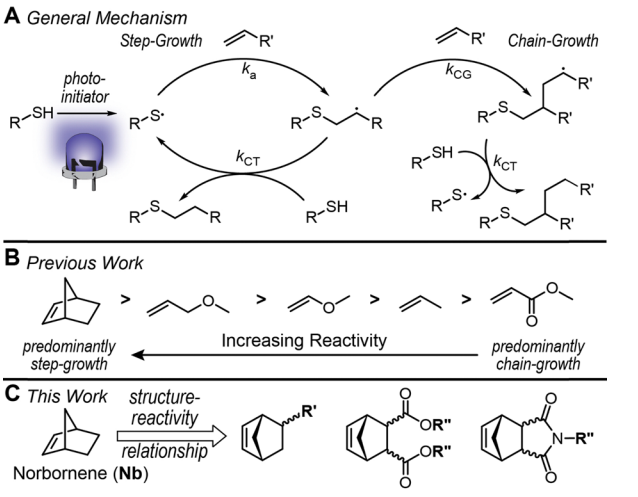

Fig. 1 Thiol–ene reaction overview. (A) General mechanism showing radical step- and chain-growth. (B) Chemical structures of enes previously examined and their relative reactivity. (C) This work on norbornene structure–reactivity relationships.

[a] *Department of Chemistry, The University of Texas at Austin, Austin, TX, USA. E-mail: zpage@utexas.edu*
[b] *McKetta Department of Chemical Engineering, The University of Texas at Austin, Austin, TX, USA*

† Electronic supplementary information (ESI) available: Materials, methods, synthesis, characterization. See DOI: https://doi.org/10.1039/d4cc06196a

transform infrared (FTIR) spectroscopy (Fig. 1C). Regio- and stereo-isomers were examined, revealing a 10-fold difference in rate between the fastest and slowest Nb substrates, which was attributed in-part to steric hindrance. Appending the most reactive Nb substrate to a hydrophilic polymer backbone showcased utility in 3D printing hydrogels.

Starting from the corresponding mixed *endo*-/*exo*-carboxylic acid or -alcohol, five Nb derivatives were synthesized bearing: methyl ester (*mix*-Nb-ester-CH_3), methylene acetate (*mix*-Nb-CH_2-acetate), acetate (*mix*-Nb-acetate), methyl ether (*mix*-Nb-ether-CH_3), or methylene methyl ether (*mix*-Nb-CH_2-ether-CH_3) (Fig. 2A). Using ^{1}H-NMR, *endo* to *exo* ratios were confirmed to range from ~3 : 2 to 4 : 1, respectively (Fig. S2, ESI†). These monofunctional derivatives were representative of precursors used to incorporate Nb into polymer scaffolds for photoinduced thiol–ene crosslinking. They are commercially supplied as *endo*/*exo* mixtures (~1.5×–4× more *endo*, Table S1, ESI†). Notably, the *exo*-carboxylic acid Nb derivative is also available, but cost prohibitive (~20× the cost of the mixed isomers), limiting its utility in applications such as 3D printing.

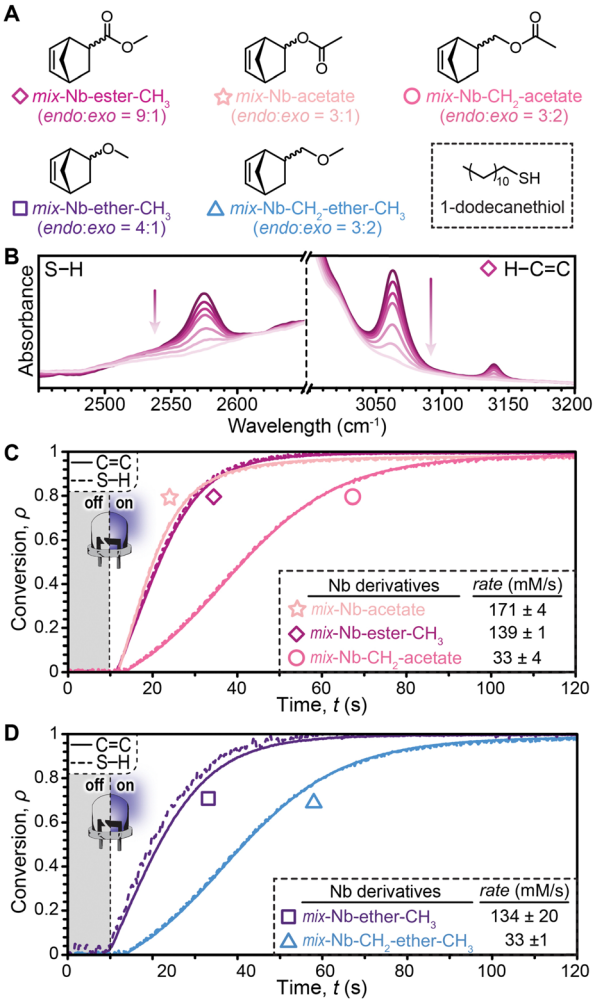

Fig. 2 Norbornene-ester and ether derivatives. (A) Chemical structures, including thiol used. (B) Representative real-time FTIR spectra for *mix*-Nb-ester-CH_3, showing both disappearance of thiol (left) and alkene (right) signals over time. (C) Summary of thiol-Nb reaction kinetics for ester and (D) ether derivatives. Samples were 100 μm thick and irradiated with a 405 nm LED (1 mW cm^{-2}).

With the mixed Nb stereoisomers, real-time FTIR spectroscopy in a transmission configuration was used to characterize photoinduced thiol–ene reactions by monitoring the disappearance of C=C–H stretches (3000–3100 cm^{-1}) and S–H stretches (2525–2625 cm^{-1}) (Fig. 2B), along with validation by monitoring the C=C stretch (~1620 cm^{-1}) on salt plates (Fig. S3, ESI†). Nb derivatives were reacted with 1-dodecanethiol (stoichiometrically balanced, neat) using phenylbis(2,4,6-trimethylbenzoyl)phosphine oxide (BAPO, 0.01 mol%) as the photoinitiator. Samples (100 μm thick) between glass slides were irradiated with a 405 nm LED (1 mW cm^{-2}), turned on 10 s after beginning each measurement. The Nb acetate and ester derivatives showed comparably high reaction rates (~170 and 140 mM s^{-1}, respectively) (Fig. 2C). Interestingly, the presence of a methylene spacer between Nb and acetate (Nb-CH_2-aceate) resulted in a ~4× slowdown (~33 mM s^{-1}). Similarly observed for the Nb-ether, a methylene spacer decreased its reactivity (Fig. 2D). The higher reactivity observed for the Nb derivatives with functionality directly attached (no CH_2 spacer) was hypothesized to arise from reduced steric interactions, although further studies are needed to elucidate the exact roles of each substituent, including the influence of electronics (*e.g.*, inductive effects), aggregation, and matrix viscosity.

Next we examined Nb-diesters and -imides, which are widely used in ring-opening metathesis polymerization (ROMP)[21,22] due to their rapid polymerization rates and ease of versatile synthesis. Four derivatives bearing 2-ethylhexyl (EH) groups were synthesized in one-step *via* substitution of inexpensive pure *endo*- or *exo*-carbic anhydride with the corresponding EH-alcohol or -amine (Fig. 3A and Schemes S6, S7, ESI†). The resulting Nb-EH derivatives were soluble in 1-dodecanethiol, enabling neat photoinitiated thiol–ene reactions.

For comparison, an analogous *mix*-Nb-ester-EH derivative was prepared and examined using real-time FTIR spectroscopy under the same conditions. Impressively, *exo*-NbI was found to be ~10× faster than the corresponding *endo*-NbI (~100 to 11 mM s^{-1}, respectively) (Fig. 2B). This trend was also observed, albeit to a lesser extent, for the Nb-diester derivatives; 43 to 17 mM s^{-1} for *exo*- and *endo*-isomers, respectively. The faster rates for the *exo*-isomers were again attributed to reduced steric hinderance of thiyl radical addition. Notably, pure *exo*-Nb-ester-EH (and –CH_3) controls deviated from this trend, with slower reactions relative to the mixed analogues (Fig. S4 and S5, ESI†). However, this was attributed to poor miscibility of the pure *exo*-isomers. Also of note was that the Nb-imide (NbI) derivatives required backgrounding with the NbI product to accurately monitor the thiol stretch at ~2600 cm^{-1} (Fig. S6 and S7, ESI†). Overall, the *exo*-NbI resulted in the fastest thiol–ene reaction, followed by the *mix*-Nb-ester-EH control at a rate of 85 mM s^{-1}.

To implement photoinduced thiol–ene crosslinking for hydrogels, we appended *exo*-NbI to poly(*N*-hydroxyethyl acrylamide) (PHEAA), which was chosen for its hydrophilicity and ease of post-functionalization. PHEAA was synthesized *via* photoiniferter polymerization[23] of HEAA in water, using a xanthate chain-transfer agent (CTA) and 8 mW cm^{-2} 365 nm LED light exposure (Fig. 4A and Fig. S10, ESI†). Targeting a degree of polymerization of 1000,

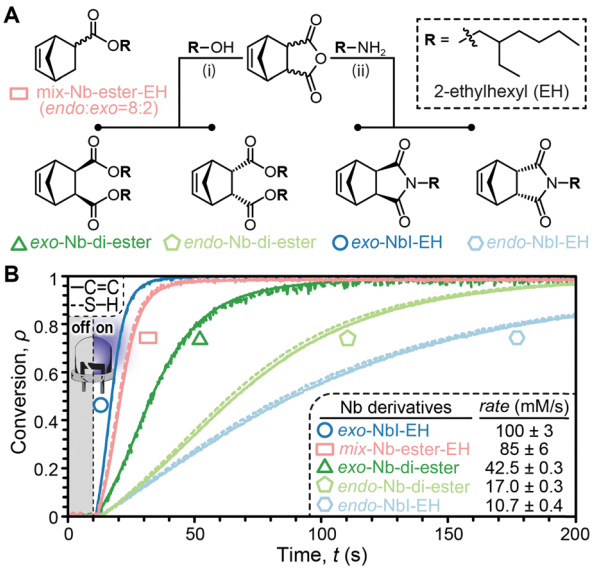

Fig. 3 Norbornene-imide and -diester derivatives bearing 2-ethylhexyl (EH) groups, relative to *mix*-Nb-ester-EH as a control. (A) Chemical structures and general synthetic protocol. Reaction conditions: (i) 2-ethylhexanol (2.2 eq.), *p*TSA (0.02 eq.), toluene, 145 °C and (ii) 2-ethylhexylamine (1.1 eq.), toluene, 145 °C. (B) Summary of thiol-Nb reaction kinetics characterized *via* real-time FTIR spectroscopy. Samples were 100 μm thick and irradiated with a 405 nm LED (1 mW cm^{-2}).

photoiniferter was rapid, reaching >95% monomer conversion in ~10 minutes. Characterizing number average molecular weight (M_n) and dispersity ($Đ$) using size exclusion chromatography (SEC) revealed that the photoiniferter polymerization was moderately controlled, as M_n increased linearly with percent monomer conversion and $Đ < 1.5$ (Fig. S11, ESI†). After precipitating PHEAA into acetone to remove unreacted monomer, *exo*-NbI bearing a glycine-linker was installed onto the sidechain *via* Steglich esterification, with a feed ratio of 10 mol% *exo*-NbI-glycine relative to HEAA repeat units. After post-functionalization, Nb-PHEAA maintained a Gaussian distribution *via* SEC, with an M_n of ~117 kDa relative to polystyrene standards (Fig. S12, ESI†). The percent Nb functionality was characterized using ^{1}H-NMR spectroscopy, revealing ~4 mol% incorporation (Fig. S13, ESI†). This synthetic protocol is versatile and scalable, providing access to "prepolymers" with tunable Nb composition and concentration (Fig. S15, ESI†).

Photoinduced crosslinking kinetics were next probed using parallel plate oscillatory shear photo-rheology. Samples contained DL-dithiothreitol (DTT) as the thiol crosslinker (~equimolar thiol to ene functionality), lithium phenyl-2,4,6-trimethylbenzoylphosphinate (LAP, 0.5 wt% ≈ 17 mM) as the water soluble photoinitiator, 2,2,6,6-tetramethyl-1-piperidinyloxy (TEMPO, 0.05 wt%) as a stabilizer, and tartrazine as a passive light absorber (*i.e.*, opaquing agent)[24] to improve 3D printing resolution (discussed later) (Fig. 4B). Irradiating this mixture in 85 wt% water (100 μm thickness) with a 405 nm LED while monitoring changes in storage (G') and loss (G'') moduli provided an estimate for the time to gelation (τ_{gel}) when $G' = G''$ (Fig. 4C). Targeting equimolar amounts of thiol and ene functional groups led to a τ_{gel} of 2.5 ± 0.1 s and 3.6 ± 0.2 s for 20 and 10 mW cm^{-2} light intensities, respectively, while a plateau G' of ~24 kPa was observed for both conditions (Table S5, ESI†). Aside from light intensity, Nb composition, Nb concentration, and

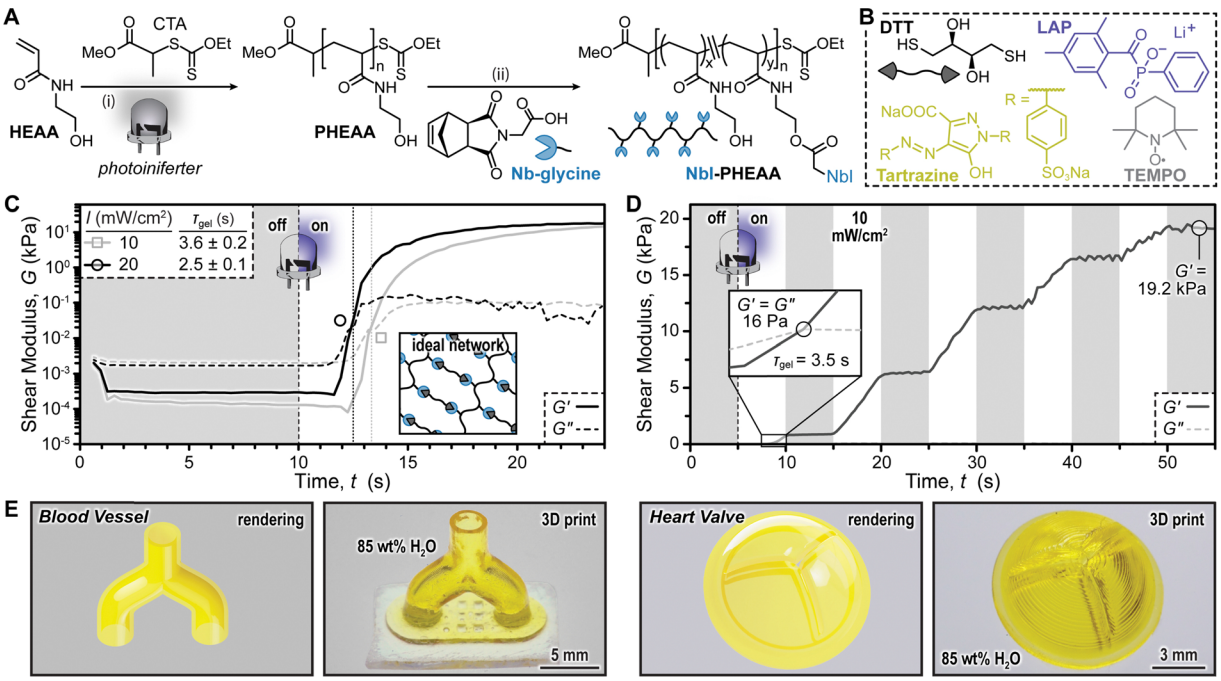

Fig. 4 Synthesis and characterization of Nb polymers and hydrogel 3D printing. (A) Photoiniferter polymerization of Nb-PHEAA and post-functionalization. Reaction conditions: (i) H_2O, 365 nm LED; (ii) EDC/HCl, DMAP, DMF. (B) Additional photocurable resin components. (C) Photo-rheology using a 405 nm LED showing the influence of light intensity and (D) temporal control with strobing the light. (E) Biomimetic 3D printed hydrogels showing both renderings and images of fabricated structures.

prepolymer M_n provided handles to alter gelation kinetics. For example, using a prepolymer that contained monofunctional Nb-ester or *endo*-NbI sidechains in-place of *exo*-NbI led to τ_{gel} values that were similar or 2× longer, respectively (Fig. S18 and Table S6, ESI†). Increasing [NbI] from ∼4 to 8 mol% resulted in a 1.4× decrease in τ_{gel}. Finally, increasing M_n from 8 to 105 kDa led to a 3× decrease in τ_{gel} (Fig. S18, S19 and Table S6, ESI†). Notably, the resins thickened over days and displayed a decrease in τ_{gel} indicative of a background reaction, common for reactive thiol–ene systems (Fig. S20, ESI†). Overall, these results demonstrate the control over gelation kinetics that the present platform offers.

To assess compatibility with DLP 3D printing we characterized the temporal control over photoinduced thiol–ene crosslinking using a resin comprising prepolymer with ∼4 mol% NbI-glycine in 85 wt% water (Fig. 4D). Cycling the 405 nm LED on/off in 10 second intervals at an intensity of 10 mW cm^{-2} revealed excellent temporal control (*i.e.*, G' increasing only while the LED was on). These results indicated that the present thiol-Nb resin might be compatible with DLP 3D printing.

As a final proof-of-concept, DLP 3D printing of the same resin was accomplished using a 405 nm LED at an intensity of 20 mW cm^{-2} (Fig. 4E). Initially, disks were printed with varying outer diameter and wall thickness under different exposure times (8–12 s/100 μm layer) to balance speed and resolution (Fig. S21 and S22, ESI†). Wall thicknesses as small as 100 μm were successfully printed and characterized with optical microscopy. Overall, the combination of speed and feature fidelity are competitive with state-of-the-art examples in thiol–ene DLP 3D printing of hydrogels (Table S7, ESI†). We then targeted several objects that contained small features and overhangs, including models of a blood vessel and heart valve (Fig. 4E), as well as a "test your printer" file (Fig. S23, ESI†) and gyroid (Fig. S24, ESI†). The bio-inspired vessel model was printed at 12 s/100 μm layer and contained hollow channels (Movie S1, ESI†). The heart valve model, printed at 6 s/100 μm, contained three leaf-like flaps to enable one-way fluid flow (Movie S2, ESI†). The successful printing of these biological models demonstrated the potential of *exo*-NbI functionality in preparing high resolution hydrogel scaffolds for biomedical applications, such as the investigation of blood flow dynamics in heart valve models.

In summary, a systematic examination of ten norbornene derivatives revealed that *exo*-NbI represents a good candidate for rapid photoinduced thiol–ene crosslinking in additive manufacturing. The influence of sterics on thiol–ene reactivity was exemplified by altering Nb stereochemistry (*exo-vs. endo-*) and mono- *vs.* di-substitution patterns, providing design principals that inform their future utility. Overall, *exo*-NbI stood out in its ease of synthetic derivatization from carbic anhydride, high thiyl radical addition rate and even higher thiol chain-transfer rate, along with its excellent spatiotemporal control in photoinduced thiol–ene crosslinking. Thus, *exo*-NbI serves as an ideal functionality to prepare polymer networks with well-defined topologies. Finally, incorporating Nb into hydrophilic polymers, such as PHEAA, was demonstrated to provide a route towards rapid light-based 3D printing of biologically relevant hydrogels that have future applications in tissue engineering.

The authors acknowledge support from the Harry S Moss Heart Trust, Bank of America, N. A., Trustee (YL, HLC, ZAP) and the Welch Foundation under Grant No. F-2007 (ZAP). Partial support was provided by the NSF Graduate Research Fellowship Program under Grant No. DGE-2137420 (EAR).

Conceptualization (YL, ZAP); methodology (YL, HLC, EAR, ZAP); investigation (YL, HLC, EAR); visualization (YL, EAR, ZAP); funding acquisition (ZAP); project administration (ZAP); supervision (ZAP); writing – original draft (YL, ZAP); writing – review & editing (YL, HLC, EAR, ZAP).

Data availability

The data supporting this article have been included as part of the ESI.†

Conflicts of interest

There are no conflicts to declare.

References

1 Y. Lv, Z. Lin and F. Svec, *Analyst*, 2012, **137**, 4114–4118.
2 A. K. Tucker-Schwartz, R. A. Farrell and R. L. Garrell, *J. Am. Chem. Soc.*, 2011, **133**, 11026–11029.
3 J. C. Grim, T. E. Brown, B. A. Aguado, D. A. Chapnick, A. L. Viert, X. Liu and K. S. Anseth, *ACS Cent. Sci.*, 2018, **4**, 909–916.
4 T. J. K. Buchner, S. Rogler, S. Weirich, Y. Armati, B. G. Cangan, J. Ramos, S. T. Twiddy, D. M. Marini, A. Weber, D. Chen, G. Ellson, J. Jacob, W. Zengerle, D. Katalichenko, C. Keny, W. Matusik and R. K. Katzschmann, *Nature*, 2023, **623**, 522–530.
5 B. D. Fairbanks, M. P. Schwartz, A. E. Halevi, C. R. Nuttelman, C. N. Bowman and K. S. Anseth, *Adv. Mater.*, 2009, **21**, 5005–5010.
6 M. Arreguín-Campos, M. Ebrahimi, A. Z. Dookhith, N. A. Lynd, G. E. Sanoja, A. A. Aldana, M. B. Baker and L. M. Pitet, *Eur. Polym. J.*, 2024, **212**, 113070.
7 B. H. Northrop and R. N. Coffey, *J. Am. Chem. Soc.*, 2012, **134**, 13804–13817.
8 N. B. Cramer, S. K. Reddy, A. K. O'Brien and C. N. Bowman, *Macromolecules*, 2003, **36**, 7964–7969.
9 T. M. Roper, C. A. Guymon, E. S. Jönsson and C. E. Hoyle, *J. Polym. Sci., Part A:Polym. Chem.*, 2004, **42**, 6283–6298.
10 S. K. Reddy, N. B. Cramer and C. N. Bowman, *Macromolecules*, 2006, **39**, 3681–3687.
11 H. Shih and C.-C. Lin, *Biomacromolecules*, 2012, **13**, 2003–2012.
12 M. H. Kim and C.-C. Lin, *ACS Appl. Mater. Interfaces*, 2023, **15**, 2737–2746.
13 W. Ma, N. Wright and Y. Wang, *ACS Macro Lett.*, 2024, **13**, 915–920.
14 K. D. Q. Nguyen, M. Crespo-Ribadeneyra, O. Picot, B. Colak and J. E. Gautrot, *ACS Appl. Polym. Mater.*, 2021, **3**, 5373–5385.
15 F.-Y. Lin and C.-C. Lin, *ACS Macro Lett.*, 2021, **10**, 341–345.
16 J. Van Hoorick, P. Gruber, M. Markovic, M. Rollot, G.-J. Graulus, M. Vagenende, M. Tromayer, J. Van Erps, H. Thienpont, J. C. Martins, S. Baudis, A. Ovsianikov, P. Dubruel and S. Van Vlierberghe, *Macromol. Rapid Commun.*, 2018, **39**, 1800181.
17 W. M. Gramlich, I. L. Kim and J. A. Burdick, *Biomaterials*, 2013, **34**, 9803–9811.
18 Z. Mũnoz, H. Shih and C.-C. Lin, *Biomater. Sci.*, 2014, **2**, 1063–1072.
19 V. T. G. Tan, D. H. T. Nguyen, R. H. Utama, M. Kahram, F. Ercole, J. F. Quinn, M. R. Whittaker, T. P. Davis and J. J. Gooding, *Polym. Chem.*, 2017, **8**, 6123–6133.
20 Y. Liu, H. L. Cater, A. J. Arrowood, G. E. Sanoja and Z. A. Page, *Macromolecules*, 2024, **57**, 6522–6530.
21 S. C. Radzinski, J. C. Foster, R. C. Chapleski, D. Troya and J. B. Matson, *J. Am. Chem. Soc.*, 2016, **138**, 6998–7004.
22 H. L. Cater, I. Balynska, M. J. Allen, B. D. Freeman and Z. A. Page, *Macromolecules*, 2022, **55**, 6671–6679.
23 R. N. Carmean, T. E. Becker, M. B. Sims and B. S. Sumerlin, *Chem*, 2017, **2**, 93–101.
24 L. M. Stevens, E. A. Recker, K. A. Zhou, V. G. Garcia, K. S. Mason, C. Tagnon, N. Abdelaziz and Z. A. Page, *Adv. Mater. Technol.*, 2023, **8**, 2300052.